



A Pseudotetrahedral Terminal Oxoiron(IV) Complex: Mechanistic Promiscuity in C–H Bond Oxidation Reactions

Katrin Warm, Alice Paskin, Uwe Kuhlmann, Eckhard Bill, Marcel Swart, Michael Haumann, Holger Dau, Peter Hildebrandt, and Kallol Ray*

Dedicated to Professor Wolfgang Kaim on the occasion of his 70th birthday

Abstract: $S=2$ oxoiron(IV) species act as reactive intermediates in the catalytic cycle of nonheme iron oxygenases. The few available synthetic $S=2$ $\text{Fe}^{\text{IV}}=\text{O}$ complexes known to date are often limited to trigonal bipyramidal and very rarely to octahedral geometries. Herein we describe the generation and characterization of an $S=2$ pseudotetrahedral $\text{Fe}^{\text{IV}}=\text{O}$ complex **2** supported by the sterically demanding 1,4,7-tri-*tert*-butyl-1,4,7-triazacyclononane ligand. Complex **2** is a very potent oxidant in hydrogen atom abstraction (HAA) reactions with large non-classical deuterium kinetic isotope effects, suggesting hydrogen tunneling contributions. For sterically encumbered substrates, direct HAA is impeded and an alternative oxidative asynchronous proton-coupled electron transfer mechanism prevails, which is unique within the nonheme oxoiron community. The high reactivity and the similar spectroscopic parameters make **2** one of the best electronic and functional models for a biological oxoiron(IV) intermediate of taurine dioxygenase (TauD-J).

Introduction

High-valent oxoiron(IV) intermediates act as the active oxidants in the catalytic cycles of a variety of mononuclear non-heme iron oxygenases.^[1] These high-valent species have been characterized by rapid freeze quench methods in few cases^[1] and were unambiguously shown by UV/Vis, Mössbauer, and X-ray absorption spectroscopic methods to contain high-spin ($S=2$) iron(IV) centres. However, the available experimental data could not reveal other important structural features, such as the number, identity, and disposition of ligands in the Fe^{IV} coordination sphere. Density functional theoretical (DFT) studies^[2] on the taurine: α KG dioxygenase

(TauD) system have shown that the spectroscopic properties of the hydrogen-abstrating oxoiron(IV) key intermediate (TauD-J) are consistent with both suggested structural models (Scheme 1), that is, with trigonal bipyramidal (*TBP*) as well as distorted octahedral (O_h) coordinations. Significant synthetic efforts in the past decade have led to the generation of oxoiron(IV) cores in both *TBP* and O_h geometries (Scheme 1). Although the majority of the synthetic complexes exhibit $S=1$ ground states in O_h geometry,^[3] DFT-studies predicted stabilization of the more reactive^[4] $S=2$ oxoiron(IV) units^[5] either by enforcing a *TBP* geometry at the iron(IV) centre^[5a–d] or by weakening the equatorial donation in O_h geometry.^[5e]

Results and Discussion

In the context of the existing ambiguity related to the coordination number of iron in biological oxoiron(IV) intermediates,^[2] and the limitation of the synthetic $S=2$ oxoiron(IV) cores to mainly *TBP* and in rare cases to O_h geometries, we have now sought to identify a tripodal ligand that allows for trapping an $\text{Fe}^{\text{IV}}=\text{O}$ core in a geometry different from the known *TBP* or O_h geometries. Herein we report the synthesis and characterization of the $S=2$ pseudotetrahedral $[\text{Fe}^{\text{IV}}(\text{O})(^t\text{Bu}_3\text{tacn})]^{2+}$ (**2**, $^t\text{Bu}_3\text{tacn}$ ^[6] = 1,4,7-tri-*tert*-butyl-1,4,7-triazacyclononane) complex, which exhibits spectroscopic and reactivity properties distinct from the oxoiron(IV) cores in *TBP* or O_h geometries. In particular, in direct contrast to the vast majority of previous oxoiron(IV) cores,^[3a–g, 5a–e] where the reactivity with substrates containing C–H bonds is controlled by the C–H bond dissociation

[*] M. Sc. K. Warm, M. Sc. A. Paskin, Prof. Dr. K. Ray
Institut für Chemie, Humboldt-Universität zu Berlin
Brook-Taylor-Str. 2, 12489 Berlin (Germany)
E-mail: kallol.ray@hu-berlin.de


Dr. U. Kuhlmann, Prof. Dr. P. Hildebrandt
Institut für Chemie, Technische Universität Berlin, Fakultät II
Straße des 17. Juni 135, 10623 Berlin (Germany)


Dr. E. Bill
Max-Planck-Institut für Chemische Energiekonversion (CEC)
Stiftstraße 34–36, 45470 Mülheim (Germany)

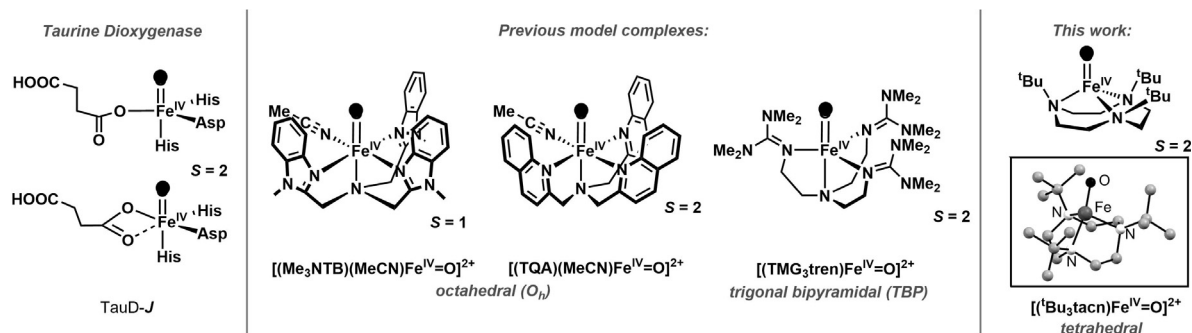
Prof. Dr. M. Swart
Institut de Química Computacional i Catàlisi, Universitat de Girona,
Campus Montilivi (Ciències)
Maria Aurèlia Capmany i Farnés, 69, 17003 Girona (Spain)

and
ICREA
Pg. Lluís Companys 23, 08010 Barcelona (Spain)

Dr. M. Haumann, Prof. Dr. H. Dau
Institut für Physik, Freie Universität Berlin
Arnimallee 14, 14195 Berlin (Germany)

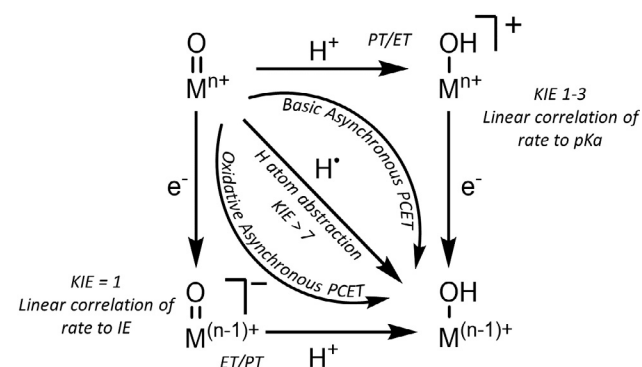
 Supporting information and the ORCID identification number(s) for the author(s) of this article can be found under:
<https://doi.org/10.1002/anie.202015896>

 © 2020 The Authors. *Angewandte Chemie International Edition* published by Wiley-VCH GmbH. This is an open access article under the terms of the Creative Commons Attribution Non-Commercial NoDerivs License, which permits use and distribution in any medium, provided the original work is properly cited, the use is non-commercial and no modifications or adaptations are made.



Scheme 1. Left: Proposed structures of $S=2$ *TauD-J* based on DFT studies;^[2] middle: selected examples of $S=1$ and $S=2$ oxoiron(IV) cores in TBP and O_h geometries; right: A pseudotetrahedral $S=2$ oxoiron(IV) complex **2** reported in this work; in the inset is shown the DFT calculated structure of **2** in the $S=2$ state.

energies (BDE_{C-H}), complex **2** demonstrates a mechanistic promiscuity in its C–H oxidation reactions. Sterically less hindered C–H bonds are oxidized via a conventional direct hydrogen atom abstraction (HAA; Scheme 2) mechanism



Scheme 2. Mechanisms of net hydrogen atom transfer.

that is characterized by large deuterium kinetic isotope effects (KIEs), which are greater than the semi-classical limit of 7, implying a significant contribution of hydrogen tunnelling.^[7] In contrast, for sterically encumbered substrates, where the direct access to the $Fe^{IV}=O$ core is blocked, the C–H oxidation reaction proceeds with a significantly lower KIE and presumably involves a proton-coupled electron transfer (PCET) mechanism along a spectrum of “asynchronicity”^[8] in which the transition state for the net H-atom transfer contains more electron transfer character (Scheme 2; Oxidative asynchronous PCET).

Combination of equimolar amounts of the previously reported tBu_3tacn ligand^[6,9] and $Fe^{II}(OTf)_2(CH_3CN)_2$ in CH_2Cl_2 afforded $[Fe^{II}(tBu_3tacn)(OTf)](OTf)$ (**1**), whose crystal structure (Figure S1; Tables S1,S2) exhibited a distorted tetrahedral geometry (N–Fe–N angles of 86.5 – 88.3°) with an Fe–O distance of $1.935(2)$ Å and three Fe–N distances of $2.105(2)$ – $2.124(2)$ Å. The zero-field Mössbauer spectrum of **1** (Figure S2) revealed a single doublet with an isomer shift (δ) of 0.97 $mm\ s^{-1}$ and a large quadrupole splitting ($\Delta E_Q = 1.98$ $mm\ s^{-1}$), consistent with an $S=2$ spin state, which is also supported by DFT^[11] (Table S3). Reaction of **1** in pure CH_2Cl_2 or butyronitrile (PrCN) at $-90^\circ C$ with 2-(*tert*-butylsulfonyl)-

iodosobenzene (tPhIO)^[12] yielded a transient species **2** (Figure 1 A; half-life at $-70^\circ C = 20$ min) with electronic absorption features centered at $\lambda_{max} = 356$ nm ($\epsilon = 7500$ $M^{-1} cm^{-1}$) and 780 nm ($\epsilon = 150$ $M^{-1} cm^{-1}$). Notably, the presence of a well-defined strong absorption band in the near-UV region is typical of $S=2$ oxoiron(IV) cores (Table S4);^[5a–d] in **2** this band at $\lambda_{max} = 356$ nm is slightly red-shifted (Table 1) relative to that of *TauD-J* ($\lambda_{max} = 318$ nm).^[1a] The $S=2$ spin state of **2** was additionally corroborated by the Evans^[13] NMR method (Figure S3) at $-90^\circ C$ which yielded the magnetic moment $\mu_{eff} = 4.50$ μ_B (theoretical value for $S=2$: 4.90 μ_B). An electron spray ionization mass spectrum (Figure S4) of **2** exhib-

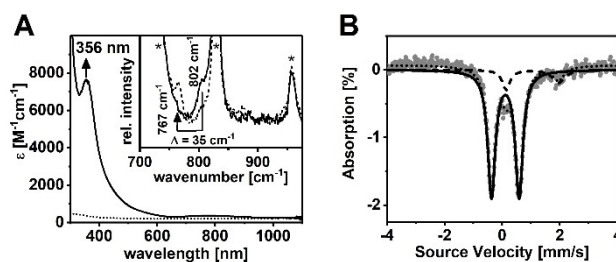


Figure 1. A) UV/Vis spectra of **1** (dashed line) and **2** (solid line) in CH_2Cl_2 at $-90^\circ C$; inset shows the rRaman spectra of ^{16}O - (solid line) and ^{18}O -labelled (dashed line) **2** (4 mM solution) in CH_2Cl_2 upon 406 nm irradiation at $-90^\circ C$; solvent signals are indicated by an asterisk; B) Zero-field Mössbauer spectrum (grey) of a frozen sample of **2** in PrCN/ CH_2Cl_2 (10:1) and simulation with $\delta = 0.11$ $mm\ s^{-1}$ and $\Delta E_Q = 0.96$ $mm\ s^{-1}$ for the main species (solid line, 87%). The minor species (dashed line) with $\delta = 0.97$ $mm\ s^{-1}$ and $\Delta E_Q = 1.98$ $mm\ s^{-1}$ corresponds to unreacted **1**.

Table 1: Comparison of the spectroscopic properties of *TauD-J* and **2**.

	<i>TauD-J</i> ^[1a,b,2,10]	2
λ_{max} [nm]	318	356
R (Fe–O) [Å]	1.62	1.66
$\nu_{Fe=O}$ [cm^{-1}]	821	802
δ [$mm^{-1} s^{-1}$]	0.31	0.11
ΔE_Q [$mm^{-1} s^{-1}$]	0.88	0.96
A_{xx}, A_{yy}, A_{zz} [T]	$S=2$: –18.4, –17.6, –31	$S=2$: –10.1, –3.3, –36.1
E_0 [eV]	7123.8	7123.2

ited a signal at $m/z = 518.7$, consistent with its formulation as $[\text{Fe}^{\text{IV}}(\text{O})(^t\text{Bu}_3\text{tacn})(\text{OTf})]^+$ (m/z calc = 518.2). However, the ^{19}F -NMR spectrum (Figure S5) of **2** displayed a single resonance at -77.0 ppm, which confirmed that the triflate (OTf) anion is not bound to the Fe-centre in **2**. This observation together with the same UV-vis spectrum (Figure S6) of **2** in both coordinating (PrCN) and non-coordinating (CH_2Cl_2) solvents corroborates the absence of any exogenous ligands binding to the iron centre. Thus, the 4-coordinate geometry found in **1** is retained in **2**, leading us to formulate the latter as $[\text{Fe}^{\text{IV}}(\text{O})(^t\text{Bu}_3\text{tacn})]^{2+}$.

The 4-coordinate geometry of **2** was also supported by Extended X-ray Absorption Fine Structure (EXAFS) analysis (Figure S7A, Table S5), which yielded a good fit with an oxygen ligand at 1.66 \AA , assigned to the Fe=O bond, and a further shell of three nitrogen ligands at 2.06 \AA , corresponding to the N donors of $^t\text{Bu}_3\text{tacn}$. The Fe K-edge X-ray absorption spectrum (Figure S7B) of **2** reveals an edge energy of 7123.2 eV (vs. 7119.7 eV for **1**), which is within the range of values found for synthetic $\text{Fe}^{\text{IV}}=\text{O}$ complexes.^[3b,5a-c] Furthermore, in contrast to the pre-edge features of existing $S=1$ complexes that can be modelled with a single Gaussian,^[13] in the pre-edge region of **2** two spectral features at ≈ 7115 and $\approx 7117 \text{ eV}$ are tentatively discernible (Figure S7A,C), which may be rationalized in terms of a splitting of the α and β d_{z^2} orbitals by spin polarization in the $S=2$ oxoiron(IV) cores.^[5a,b]

Resonance Raman spectroscopy revealed a $\nu(\text{Fe}=\text{O})$ stretching mode at 802 cm^{-1} in **2** (Figure 1A, inset) that shifted to 767 cm^{-1} upon ^{18}O -labelling. The observed $\nu(\text{Fe}=\text{O})$ mode has one of the lowest energies reported to date for oxoiron(IV) cores. This may be attributed to the high spin ($S=2$) ground state of **2** as this would (in a simplified pseudotetrahedral ligand field) require a $d(x^2-y^2)^1d(xy)^1d(xz,yz)^2d(z^2)^0$ electronic configuration with an Fe–O bond order (BO) of 2.0 .^[15] Notably, the high-spin ground state of **2** is unique for a pseudotetrahedral geometry; previously reported pseudotetrahedral M–X ($X = \text{O}^{2-}$, NR^{2-} , or N^{3-}) complexes,^[16] including the recent $\text{Co}^{\text{III}}=\text{O}$ complex,^[8,17] all possess a low-spin ground state with a M–X BO of 3 . The zero field Mössbauer spectrum of **2** exhibits a doublet (87% yield) with a quadrupole splitting, $\Delta E_Q = 0.96 \text{ mm s}^{-1}$, and an isomer shift, $\delta = 0.11 \text{ mm s}^{-1}$ (Figure 1B). Although, the ΔE_Q value is very close to the value reported for TauD-J (Table 1),^[1b] the δ -value is significantly lower, which may reflect the nitrogen-rich character in **2** in contrast to the harder oxygen-containing ligand sphere in TauD-J. In applied magnetic fields, the spectra of **2** exhibit paramagnetic hyperfine structures, which were analysed by assuming an $S=2$ center yielding a non-axial A-tensor with $A_{xx}/g_n\beta_n = -10.1 \text{ T}$, $A_{yy}/g_n\beta_n = -3.3 \text{ T}$ and $A_{zz}/g_n\beta_n = -36.1 \text{ T}$ (Figure S8). The structure of **2** as obtained by DFT calculations (Scheme 1, inset) reveals an off-axis tilt of the oxo ligand resulting in a deviation from the C_3 symmetry, which may account for the non-axial A-tensor determined from magnetic Mössbauer studies. The quintet state was calculated to be more stable than the triplet and the singlet states by 0.8 and $6.6 \text{ kcal mol}^{-1}$, respectively (Table S3). Furthermore, among all spin states, the calculated spectroscopic properties of the $S=2$ state provide the best

description of the experimental data. The calculated Fe=O and Fe–N bond distances (1.63 and 2.06 \AA , respectively), Fe=O stretching mode frequency (893 cm^{-1} , ^{18}O isotope shift -36 cm^{-1}), and Mössbauer δ -value (0.06 mm s^{-1}), on the ground $S=2$ state are in satisfactory agreement with experiments (Table S3). Notably, the calculated data for the $S=1$ and $S=0$ states deviate significantly from the experiments, such that we take the calculations as a further support for the $S=2$ ground state in **2**.

The oxidative reactivity of **2** (Figures S9–S18; Table S6) has been investigated with several substrates in oxygen atom transfer (OAT) and HAA reactions and the second order rate constants derived from these studies in CH_2Cl_2 are compared with three of the most reactive high-valent Fe-oxo intermediates reported to date (namely the $[(\text{TQA})\text{Fe}^{\text{IV}}(\text{O})(\text{CH}_3\text{CN})]^{2+}$ (TQA = tris(2-quinolylmethyl)amine),^[5c] $[(\text{Me}_3\text{NTB})\text{Fe}^{\text{IV}}(\text{O})]^{2+}$ (Me_3NTB = tris((N-methyl-benzimidazol-2-yl)methyl)amine)^[3c] and $[(\text{TMCO})\text{Fe}^{\text{IV}}(\text{O})(\text{CH}_3\text{CN})]^{2+}$ (TMCO = 4,8,12-trimethyl-1-oxa-4,8,12-triazacyclotetradecane)^[3f] complexes (Table 2). In reactions with ethylbenzene, 1,4-cyclohexadiene (1,4-CHD), and toluene, **2**

Table 2: Comparison of the reaction rate constants k_2' (normalized to the number of equivalent H atoms) at -40°C for the C–H activation reaction of **2** and the highly reactive intermediates $(\text{TMCO})\text{Fe}^{\text{IV}}=\text{O}$, $(\text{Me}_3\text{NTB})\text{Fe}^{\text{IV}}=\text{O}$ and $(\text{TQA})\text{Fe}^{\text{IV}}=\text{O}$ towards a selection of substrates.

Substrate ($\text{BDE}_{\text{C-H}}$, kcal/mol)	k_2' [$\text{M}^{-1} \text{ s}^{-1}$]			
2	(TMCO) $\text{Fe}^{\text{IV}}=\text{O}$	(Me_3NTB) $\text{Fe}^{\text{IV}}=\text{O}$	(TQA) $\text{Fe}^{\text{IV}}=\text{O}$	
1,4-CHD (76.0)	$1.0 \times 10^{2[a]}$	nd	7.8×10^2	nd
DHA (76.3)	$1.6^{[b]}$	Too fast (-90°C)	2.4×10^2	nd
Ethylbenzene (85.4)	$3.3^{[b]}$	$0.10^{[c]}$	0.75	1.1
Toluene (89.7)	$0.43^{[b]}$	$0.0044^{[d]}$	0.16	0.21

nd = rate not determined; k_2' values at -40°C were calculated from the values measured at [a] -90°C ; [b] -70°C ; [c] -60°C ; [d] -50°C and corrected for the temperature difference by doubling the rate for every 10 degrees rise in temperature.

is a stronger oxidant than $[(\text{TMCO})\text{Fe}^{\text{IV}}(\text{O})(\text{CH}_3\text{CN})]^{2+}$, but comparable to $[(\text{TQA})\text{Fe}^{\text{IV}}(\text{O})(\text{CH}_3\text{CN})]^{2+}$ and $[(\text{Me}_3\text{NTB})\text{Fe}^{\text{IV}}(\text{O})]^{2+}$. Interestingly, the reactivity trend is reversed in reactions with 9,10-dihydroanthracene (DHA), where **2** exhibits the least reactivity. Furthermore, when the logarithms of the statistically corrected second order rate constants (k_2') were plotted vs. the $\text{BDE}_{\text{C-H}}$ values of the substrates (Figure 2A, Figure S20A), the linear correlation typically observed for oxoiron(IV) cores^[3a-i,5] is found to be not valid for **2**. While the respective $\log(k_2')$ values associated with **2** for the oxidation of 1,4-CHD, 1,3-cyclohexadiene (1,3-CHD), ethylbenzene, cyclohexene and toluene fall on a line (Figure 2A, black points), xanthene, DHA, indene and fluorene substrates (Figure 2A, inset) deviate from this pattern and exhibit significantly lower rates than predicted by the linear relationship. Particularly interesting is the large rate difference of two orders of magnitude for DHA and 1,4-CHD, which are known to have small difference in $\text{BDE}_{\text{C-H}}$ values.^[18] Furthermore, large deuterium KIEs of 7 (Figure S9), 12 (Figure S10), and 53 (Figure 2C, Figure S11) were

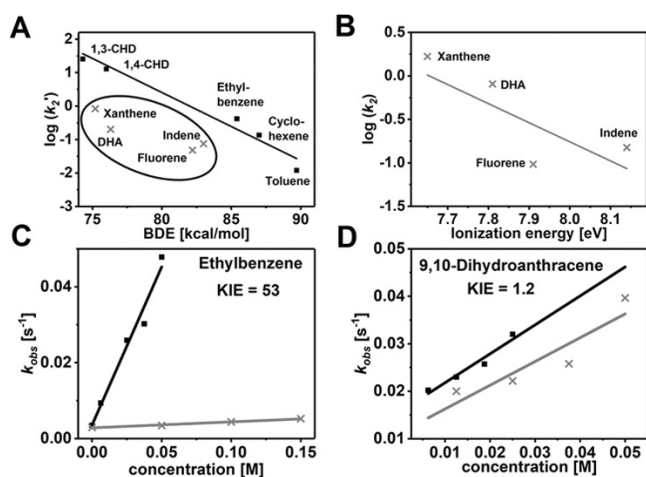


Figure 2. A) Plot of the logarithm of the second order rate constants k_2' (normalized to the number of equivalent H atoms) of the reactions of **2** with different substrates vs. the BDE_{C-H} of the respective substrates; the inset shows the substrates that deviate from a linear correlation; B) Plot of the logarithm of the second order rate constants k_2 of the reactions of **2** with different polycyclic substrates vs. the ionization energy of the respective substrates; C) plot of the first-order rate constants k_{obs} vs. the concentration of ethylbenzene (black) and d_{10} -ethylbenzene (grey) for determination of the second-order rate constants k_2 and the deuterium KIE; D) plot of the first-order rate constants k_{obs} vs. the concentration of DHA (black) and d_4 -DHA (grey) for determination of the second-order rate constant k_2 and the deuterium KIE.

recorded for toluene, 1,4-CHD, and ethylbenzene reactions, respectively, suggesting a HAA mechanism with significant contribution of hydrogen-tunnelling, as is frequently proposed in C–H bond activation reactions of $Fe^{IV}=O$ species.^[7] In contrast, significantly reduced *KIEs* of 1.2 (Figure 2D, Figure S12) and 2.1 (Figure S13) were determined for DHA and xanthene, respectively, thereby pointing to a change of mechanism. Further mechanistic insights were obtained by plotting the rate constants against the pK_a and the ionization energies (IE) of the substrates. The $\log(k_2)$ vs. IE plot (Figure 2B, Figure S20B) revealed that for reactions of **2** with xanthene, DHA, indene and fluorene the rate decreased linearly with increasing IE, whereas the rates for 1,4-CHD, 1,3-CHD, ethylbenzene, cyclohexene and toluene scatter irregularly. Furthermore, no linear trend was observed in the $\log(k_2)$ vs. pK_a plot (Figure S20C) for all the investigated substrates. Thus, the tBu_3tacn ligand blocks the HAA pathway by presumably impeding access of the bulkier polycyclic hydrocarbons to the $Fe=O$ unit in **2**. An alternative oxidative asynchronous PCET mechanism (Scheme 2) prevails in such cases, which are typically characterized by low *KIEs* and a linear correlation of the reaction rates to IEs.

Conclusion

Taken together the results presented herein unequivocally validate the formation of a terminal oxoiron(IV) complex **2** in a pseudotetrahedral geometry. The computational and experimental analyses are consistent with the presence of an $S=$

2 $Fe^{IV}=O$ core in **2**. Complex **2** represents the only example of a high-spin complex with metal-ligand multiple bond character in a pseudotetrahedral geometry; notably, a pseudotetrahedral oxoiron(IV) complex has been very recently demonstrated to possess an $S=0$ state in the gas-phase.^[19] The absorption spectrum, Mössbauer ΔE_Q , Fe K-edge energy, and the $\nu(Fe=O)$ mode of **2** (Table 1) bear very close resemblance to the corresponding spectroscopic properties of TauD-**J**. **2** also exhibits the distinct high-reactivity features known from the strongly oxidizing iron-oxo cores in biology and accordingly possesses one of the most reactive oxoiron(IV) cores that have been synthesized to date. Furthermore, a large *KIE* of 53 has been determined for the reaction of **2** with ethylbenzene, which compares well with the *KIE* of 57^[1] determined for the oxidation of taurine by TauD-**J**. The uniqueness of **2** within the non-heme oxoiron family is, however, emphasized in its ability to oxidize sterically hindered C–H bonds by an IE-driven asynchronous PCET mechanism. Although limited examples of C–H oxidation by a basicity controlled PCET mechanism (Scheme 2) are known,^[8,20] evidence of oxidative PCET mechanism has stayed elusive prior to this study. In conclusion, the high reactivity and the similar spectroscopic parameters of **2** and TauD-**J** make **2** one of the best structural, electronic and functional models for TauD-**J**.

Acknowledgements

This work was funded by the Deutsche Forschungsgemeinschaft (DFG, German Research Foundation) under Germany's Excellence Strategy—EXC 2008–390540038—UniSys-Cat to K.R., P.H., and H.D., and the Heisenberg-Professorship to K.R., and MINECO (CTQ2017-87392-P) and FED-ER (UNGI10-4E-801) to M.S. K.W. also thanks Einstein Foundation Berlin (ESB)—Einstein Center of Catalysis (EC²) for its support. Open access funding enabled and organized by Projekt DEAL.

Conflict of interest

The authors declare no conflict of interest.

Keywords: bioinorganic chemistry · enzyme models · high-valent iron · hydrogen atom abstraction · electron transfer

- [1] a) J. C. Price, E. W. Barr, B. Tirupati, J. M. Bollinger, C. Krebs, *Biochemistry* **2003**, *42*, 7497–7508; b) J. M. Bollinger, Jr., J. C. Price, L. M. Hoffart, E. W. Barr, C. Krebs, *Eur. J. Inorg. Chem.* **2005**, 4245–4254; c) C. Krebs, D. Galonić Fujimori, C. T. Walsh, J. M. Bollinger, *Acc. Chem. Res.* **2007**, *40*, 484–492.
- [2] S. Sinnecker, N. Svensen, E. W. Barr, S. Ye, J. M. Bollinger, F. Neese, C. Krebs, *J. Am. Chem. Soc.* **2007**, *129*, 6168–6179.
- [3] a) C. A. Grapperhaus, B. Mienert, E. Bill, T. Weyhermüller, K. Wieghardt, *Inorg. Chem.* **2000**, *39*, 5306–5317; b) J.-U. Rohde, J.-H. In, M. H. Lim, W. W. Brennessel, M. R. Bukowski, A. Stubna, E. Münck, W. Nam, L. Que, *Science* **2003**, *299*, 1037; c) M. S. Seo, N. H. Kim, K.-B. Cho, J. E. So, S. K. Park, M. Clémancey, R. Garcia-Serres, J.-M. Latour, S. Shaik, W. Nam, *Chem. Sci.* **2011**,

- 2, 1039–1045; d) S. Meyer, I. Klawitter, S. Demeshko, E. Bill, F. Meyer, *Angew. Chem. Int. Ed.* **2013**, *52*, 901–905; *Angew. Chem.* **2013**, *125*, 935–939; e) D. Wang, K. Ray, M. J. Collins, E. R. Farquhar, J. R. Frisch, L. Gómez, T. A. Jackson, M. Kerscher, A. Waleska, P. Comba, M. Costas, L. Que, *Chem. Sci.* **2013**, *4*, 282–291; f) I. Monte Pérez, X. Engelmann, Y.-M. Lee, M. Yoo, E. Kumaran, E. R. Farquhar, E. Bill, J. England, W. Nam, M. Swart, K. Ray, *Angew. Chem. Int. Ed.* **2017**, *56*, 14384–14388; *Angew. Chem.* **2017**, *129*, 14576–14580; g) J. B. Gordon, A. C. Vilbert, I. M. DiMucci, S. N. MacMillan, K. M. Lancaster, P. Moënnelocoz, D. P. Goldberg, *J. Am. Chem. Soc.* **2019**, *141*, 17533–17547; h) W. Nam, *Acc. Chem. Res.* **2015**, *48*, 2415–2423; i) V. A. Larson, B. Battistella, K. Ray, N. Lehnert, W. Nam, *Nat. Rev. Chem.* **2020**, *4*, 404–419; j) X. Engelmann, I. Monte-Pérez, K. Ray, *Angew. Chem. Int. Ed.* **2016**, *55*, 7632–7649; *Angew. Chem.* **2016**, *128*, 7760–7778; k) J. J. D. Sacramento, D. P. Goldberg, *Acc. Chem. Res.* **2018**, *51*, 2641–2652; l) J. Chen, Z. Jiang, S. Fukuzumi, W. Nam, B. Wang, *Coord. Chem. Rev.* **2020**, *421*, 213443; m) M. Guo, T. Corona, K. Ray, W. Nam, *ACS Cent. Sci.* **2019**, *5*, 13–28; n) L. Que, *Acc. Chem. Res.* **2007**, *40*, 493–500; o) A. R. McDonald, L. Que, Jr., *Coord. Chem. Rev.* **2013**, *257*, 414–428.
- [4] a) S. Shaik, H. Hirao, D. Kumar, *Acc. Chem. Res.* **2007**, *40*, 532–542; b) L. Bernasconi, M. J. Louwerse, E. J. Baerends, *Eur. J. Inorg. Chem.* **2007**, 3023–3033; c) A. Decker, J.-U. Rohde, E. J. Klinker, S. D. Wong, L. Que, E. I. Solomon, *J. Am. Chem. Soc.* **2007**, *129*, 15983–15996; d) C. Geng, S. Ye, F. Neese, *Angew. Chem. Int. Ed.* **2010**, *49*, 5717–5720; *Angew. Chem.* **2010**, *122*, 5853–5856.
- [5] a) J. England, Y. Guo, K. M. Van Heuvelen, M. A. Cranswick, G. T. Rohde, E. L. Bominaar, E. Münck, L. Que, *J. Am. Chem. Soc.* **2011**, *133*, 11880–11883; b) J. England, M. Martinho, E. R. Farquhar, J. R. Frisch, E. L. Bominaar, E. Münck, L. Que, Jr., *Angew. Chem. Int. Ed.* **2009**, *48*, 3622–3626; *Angew. Chem.* **2009**, *121*, 3676–3680; c) D. C. Lacy, R. Gupta, K. L. Stone, J. Greaves, J. W. Ziller, M. P. Hendrich, A. S. Borovik, *J. Am. Chem. Soc.* **2010**, *132*, 12188–12190; d) J. P. Bigi, W. H. Harman, B. Lassalle-Kaiser, D. M. Robles, T. A. Stich, J. Yano, R. D. Britt, C. J. Chang, *J. Am. Chem. Soc.* **2012**, *134*, 1536–1542; e) A. N. Biswas, M. Puri, K. K. Meier, W. N. Oloo, G. T. Rohde, E. L. Bominaar, E. Münck, L. Que, *J. Am. Chem. Soc.* **2015**, *137*, 2428–2431; f) M. Puri, L. Que, *Acc. Chem. Res.* **2015**, *48*, 2443–2452.
- [6] A. Thangavel, M. Wieliczko, J. Bacsa, C. C. Scarborough, *Inorg. Chem.* **2013**, *52*, 13282–13287.
- [7] a) D. Mandal, S. Shaik, *J. Am. Chem. Soc.* **2016**, *138*, 2094–2097; b) D. Mandal, D. Mallick, S. Shaik, *Acc. Chem. Res.* **2018**, *51*, 107–117; c) E. J. Klinker, S. Shaik, H. Hirao, L. Que, Jr., *Angew. Chem. Int. Ed.* **2009**, *48*, 1291–1295; *Angew. Chem.* **2009**, *121*, 1317–1321.
- [8] M. K. Goetz, J. S. Anderson, *J. Am. Chem. Soc.* **2019**, *141*, 4051–4062.
- [9] G. J. Karahalios, A. Thangavel, B. Chica, J. Bacsa, R. B. Dyer, C. C. Scarborough, *Inorg. Chem.* **2016**, *55*, 1102–1107.
- [10] P. J. Riggs-Gelasco, J. C. Price, R. B. Guyer, J. H. Brehm, E. W. Barr, J. M. Bollinger, C. Krebs, *J. Am. Chem. Soc.* **2004**, *126*, 8108–8109.
- [11] a) M. Swart, M. Gruden, *Acc. Chem. Res.* **2016**, *49*, 2690–2697; b) M. Swart, *Chem. Phys. Lett.* **2013**, *580*, 166–171.
- [12] D. Macikenas, E. Skrzypczak-Jankun, J. D. Protasiewicz, *J. Am. Chem. Soc.* **1999**, *121*, 7164–7165.
- [13] D. F. Evans, *J. Chem. Soc. (Resumed)* **1959**, 2003–2005.
- [14] T. A. Jackson, J.-U. Rohde, M. S. Seo, C. V. Sastri, R. DeHont, A. Stubna, T. Ohta, T. Kitagawa, E. Münck, W. Nam, L. Que, *J. Am. Chem. Soc.* **2008**, *130*, 12394–12407.
- [15] J. F. Berry, S. DeBeer George, F. Neese, *Phys. Chem. Chem. Phys.* **2008**, *10*, 4361–4374.
- [16] a) T. A. Betley, J. C. Peters, *J. Am. Chem. Soc.* **2003**, *125*, 10782–10783; b) X. Hu, K. Meyer, *J. Am. Chem. Soc.* **2004**, *126*, 16322–16323; c) R. E. Cowley, R. P. Bontchev, J. Sorrell, O. Sarracino, Y. Feng, H. Wang, J. M. Smith, *J. Am. Chem. Soc.* **2007**, *129*, 2424–2425; d) C. T. Saouma, J. C. Peters, *Coord. Chem. Rev.* **2011**, *255*, 920–937; e) B. Wu, R. Hernández Sánchez, M. W. Bezpalko, B. M. Foxman, C. M. Thomas, *Inorg. Chem.* **2014**, *53*, 10021–10023; f) D. T. Shay, G. P. A. Yap, L. N. Zakharov, A. L. Rheingold, K. H. Theopold, *Angew. Chem. Int. Ed.* **2005**, *44*, 1508–1510; *Angew. Chem.* **2005**, *117*, 1532–1534; g) J. J. Scepaniak, C. S. Vogel, M. M. Khusniyarov, F. W. Heinemann, K. Meyer, J. M. Smith, *Science* **2011**, *331*, 1049–1052; h) K. Ray, F. Heims, F. F. Pfaff, *Eur. J. Inorg. Chem.* **2013**, 3784–3807.
- [17] M. K. Goetz, E. A. Hill, A. S. Filatov, J. S. Anderson, *J. Am. Chem. Soc.* **2018**, *140*, 13176–13180.
- [18] a) Y.-R. Luo, *Comprehensive Handbook of Chemical Bond Energies*, CRC, Boca Raton, **2007**; b) J. E. M. N. Klein, B. Dereli, L. Que, Jr., C. J. Cramer, *Chem. Commun.* **2016**, *52*, 10509–10512.
- [19] E. Andris, K. Segers, J. Mehara, L. Rulíšek, J. Roithová, *Angew. Chem. Int. Ed.* **2020**, *59*, 23137–23144.
- [20] a) D. Usharani, D. C. Lacy, A. S. Borovik, S. Shaik, *J. Am. Chem. Soc.* **2013**, *135*, 17090–17104; b) T. H. Parsell, M.-Y. Yang, A. S. Borovik, *J. Am. Chem. Soc.* **2009**, *131*, 2762–2763.

Manuscript received: November 29, 2020

Accepted manuscript online: December 21, 2020

Version of record online: February 15, 2021